

Neuron

Selective Optogenetic Control of Purkinje Cells in Monkey Cerebellum

Highlights

- An L7 promoter in AAV vectors restricted ChR2 expression to macaque Purkinje cells
- Sinusoidal illumination of ChR2+ cells drove vigorous, entrained spiking responses
- Activation of Purkinje cells in the oculomotor vermis biased saccade trajectories

Authors

Yasmine El-Shamayleh,
Yoshiko Kojima, Robijanto Soetedjo,
Gregory D. Horwitz

Correspondence

ghorwitz@u.washington.edu

In Brief

Manipulating the activity of specific neuronal types has been difficult in primates. El-Shamayleh et al. achieve selective optogenetic activation of Purkinje cells in the macaque cerebellum via AAV-mediated delivery of the ChR2 gene under control of an L7 promoter.



Selective Optogenetic Control of Purkinje Cells in Monkey Cerebellum

Yasmine El-Shamayleh,^{1,2} Yoshiko Kojima,^{1,2} Robijanto Soetedjo,^{1,2} and Gregory D. Horwitz^{1,2,3,*}

¹Department of Physiology & Biophysics

²Washington National Primate Research Center

University of Washington, 1959 NE Pacific St., HSB I-728, UW Mailbox 357290, Seattle, WA 98195, USA

³Lead Contact

*Correspondence: ghorwitz@u.washington.edu

<http://dx.doi.org/10.1016/j.neuron.2017.06.002>

SUMMARY

Purkinje cells of the primate cerebellum play critical but poorly understood roles in the execution of coordinated, accurate movements. Elucidating these roles has been hampered by a lack of techniques for manipulating spiking activity in these cells selectively—a problem common to most cell types in non-transgenic animals. To overcome this obstacle, we constructed AAV vectors carrying the channelrhodopsin-2 (ChR2) gene under the control of a 1 kb L7/Pcp2 promoter. We injected these vectors into the cerebellar cortex of rhesus macaques and tested vector efficacy in three ways. Immunohistochemical analyses confirmed selective ChR2 expression in Purkinje cells. Neurophysiological recordings confirmed robust optogenetic activation. Optical stimulation of the oculomotor vermis caused saccade dysmetria. Our results demonstrate the utility of AAV-L7-ChR2 for revealing the contributions of Purkinje cells to circuit function and behavior, and they attest to the feasibility of promoter-based, targeted, genetic manipulations in primates.

INTRODUCTION

The cerebellum is a phylogenetically conserved brain structure composed of distinct cell types connected by stereotyped circuitry. Purkinje cells, the sole output of the cerebellar cortex, are involved in the execution of accurate and well-timed movements (Holmes, 1939; Robinson and Fuchs, 2001; Thach et al., 1992; Wolpert et al., 1998), balance and posture (Ioffe, 2013; Morton and Bastian, 2004), and learning and memory (Ito, 2002; Raymond et al., 1996). How Purkinje cells contribute to these capacities is poorly understood in large part because techniques for manipulating activity in these cells selectively are unavailable in most animal models. The inability to target these cells in non-human primates has been particularly limiting because these animals possess a combination of fine motor control, behavioral consistency, and trainability that make them particularly well suited for testing some hypotheses of Purkinje cell function.

Purkinje cell activity can be manipulated without directly affecting other cell types using optogenetics. In transgenic animals, cell-type-specific targeting is relatively straightforward and requires genetic modifications early in development (for a review, see Stugocka et al., 2017). In non-transgenic animals, however, targeting is difficult. The difficulty arises from the method of gene delivery—typically viral vector injection into adult animals. These vectors carry promoter sequences that can confer a degree of cell-type specificity, but this specificity is usually modest (Kügler, 2015). Recently however, a cell-type-specific promoter was used to express channelrhodopsin-2 (ChR2) selectively in dopamine neurons of rhesus macaques (Stauffer et al., 2016). Optical stimulation of these neurons produced spiking activity and caused the monkeys to make behavioral responses that they learned, over repeated trials, would trigger additional optical stimulation. Targeted ChR2 expression was achieved with an intersectional, dual-vector strategy in which one vector carried the gene for the enzyme Cre recombinase under the control of the tyrosine hydroxylase promoter (TH) and the other carried the gene for ChR2 in the FLExed (Cre-dependent) configuration (Schnütgen et al., 2003). This strategy ensured that only neurons in which the TH promoter was active produced Cre recombinase, catalyzing ChR2 expression in dopaminergic neurons selectively.

Motivated by this advance and the quest for a generalizable strategy for targeting gene delivery to specific primate neuronal types, we addressed three open questions. First, can cell-type-specific promoters delivered by viral vector drive physiological levels of opsin expression directly—without a Cre-dependent strategy? A single vector strategy, if sufficiently selective, would be simpler and more efficient. Second, can cell-type specificity be achieved with a single promoter when packaged in different vector serotypes? Knowing the extent to which cell-type specificity is mediated by the promoter, as opposed to vector serotype, is critical for assessing the generalizability of this approach. Third, are cell-type-specific optogenetic manipulations sufficient to affect primate behavior on single trials? Knowing the time course over which optical stimulation affects behavior constrains the set of hypotheses that can be tested with this technique.

To answer these questions, we expressed ChR2 in Purkinje cells of rhesus macaques using an adeno-associated viral vector (AAV) containing a 1 kb fragment of the murine L7/Pcp2 promoter (Iida et al., 2013; Oberdick et al., 1990; Tsubota et al., 2011; Yoshihara et al., 1999). We used a single vector approach

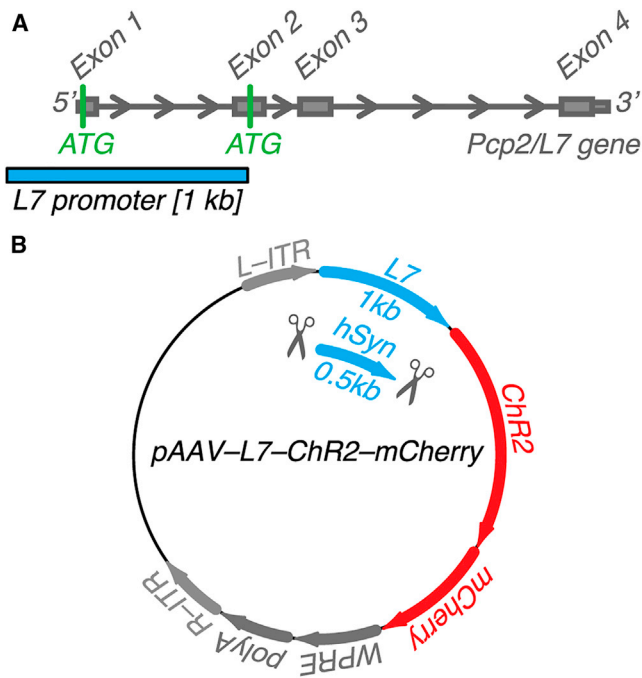


Figure 1. AAV Plasmid Cloning

(A) The L7/Pcp2 promoter fragment is shown in relation to the L7/Pcp2 gene model; this fragment corresponds to the 1 kb sequence upstream of the ATG in exon 2.

(B) The L7/Pcp2 promoter was cloned upstream of the channelrhodopsin-2 (ChR2(H143R)) and mCherry coding sequences, replacing the human synapsin promoter (hSyn, 0.5 kb).

that did not require Cre-dependent recombination, and we varied the vector serotype (AAV9 and AAV1). Histological analyses confirmed Purkinje cell-specific ChR2 expression with both serotypes. Sinusoidal optical stimulation evoked vigorous, entrained spiking responses. Optical stimulation of the oculomotor vermis, triggered by saccade initiation, exerted significant and consistent effects on saccade trajectories with a latency of ~15 ms. These results demonstrate the utility of the AAV-L7-ChR2 vector for investigating the contributions of Purkinje cells to circuit function and behavior in primates, and they confirm that short promoters can mediate cell-type-specific opsin expression at physiological levels in non-transgenic animals.

RESULTS

To excite Purkinje cells selectively, we engineered AAV vectors containing a 1 kb fragment of the L7/Pcp2 promoter upstream of the channelrhodopsin-2 gene (ChR2(H143R)) and injected them into the cerebellar cortex of three rhesus macaques (Figure 1). Below, we show that ChR2 expression was restricted to Purkinje cells and was sufficiently strong to mediate optically driven changes in spiking activity and saccade metrics.

Specificity of Vector-Mediated Expression

We injected two monkeys (monkey 1 and monkey 2) with AAV9-L7-ChR2-mCherry. After conducting neurophysiological experiments, we processed their cerebella immunohistochemically to

identify transduced cells based on mCherry expression (Figures 2A–2D). Almost all mCherry-positive cells (red) were Purkinje cells as assessed by morphology, position in the Purkinje cell layer, and expression of calbindin (green), a reliable Purkinje cell marker (Fortin et al., 1998; Jande et al., 1981; Whitney et al., 2008). In contrast, few other cells were mCherry positive (Figures S1A and S1B).

We quantified the selectivity and efficiency of the AAV9-L7-ChR2-mCherry vector by counting the number of mCherry-positive and calbindin-positive cells in three histological sections within the region of strongest expression (Figure 3). Selectivity, defined as the percentage of mCherry-positive cells that were also calbindin positive, was consistently high across sections and monkeys: $91\% \pm 1\%$ for monkey 1 and $96\% \pm 2\%$ for monkey 2 (mean \pm SE; Figure 3C, red). Efficiency, defined as the percentage of calbindin-positive cells over the counting region that were also mCherry positive, was also consistently high: $72\% \pm 6\%$ for monkey 1 and $83\% \pm 3\%$ for monkey 2 (mean \pm SE; Figure 3C, green). Together, these analyses show that most of the transduced cells near the injection site were Purkinje cells and that most Purkinje cells near the injection site were transduced. We inspected 16 cells that were mCherry positive and not calbindin positive by confocal microscopy (63 \times). These cells were all located in the granule cell layer and had granule cell-like morphology (see Figure S1; images in regions corresponding to black boxes in Figures 3A and 3B).

We injected monkey 2 with two AAV serotypes—1 and 9—containing the same L7-ChR2 construct, allowing us to compare the selectivity and efficiency of these serotypes in the same animal (Figure S2). AAV1 and AAV9 vectors had similar selectivity, both $96\% \pm 2\%$ (mean \pm SE; Figure 3C, red), but the AAV1 vector had an efficiency of only $49\% \pm 3\%$ (mean \pm SE; Figure 3C, green), possibly related to previous AAV1 injections made in this animal (Calcedo and Wilson, 2013; Mendoza et al., 2017, see data for monkey F in their Figure 6). These analyses demonstrate that Purkinje cell-specific expression of ChR2 can be achieved with either AAV1 or AAV9 vectors.

We considered the possibility that, despite their evolutionary divergence (Gao et al., 2004), AAV1 and AAV9 share a natural tropism for Purkinje cells irrespective of the promoter they carry. To control for this possibility, we injected monkey 3 with AAV1-CMV-GFP, a vector driving the expression of green fluorescent protein (GFP) under control of the cytomegalovirus (CMV) promoter, which we expected to transduce cerebellar cell types less selectively (Figure 4). In this monkey, GFP expression was observed in granule cells (Figure 4A, upper white box; Figure S3A, arrows), glia (Figure 4B, lower white box; Figure S3B), and Golgi cells (Figure S3C), in addition to Purkinje cells (Figure 4B; region corresponding to middle white box in Figure 4A). Only 8% of GFP-positive cells were Purkinje cells (Figure 4C). This non-selective expression pattern shows that the Purkinje cell specificity of the AAV1-L7-ChR2 vector was not due to the AAV1 capsid.

Optogenetic Activation of Purkinje Cells

We measured responses to blue (450 nm) light delivered via optical fiber to the cerebellar cortex. At sites where optically driven responses were evoked, we varied the frequency of

AAV9-L7-ChR2-mCherry

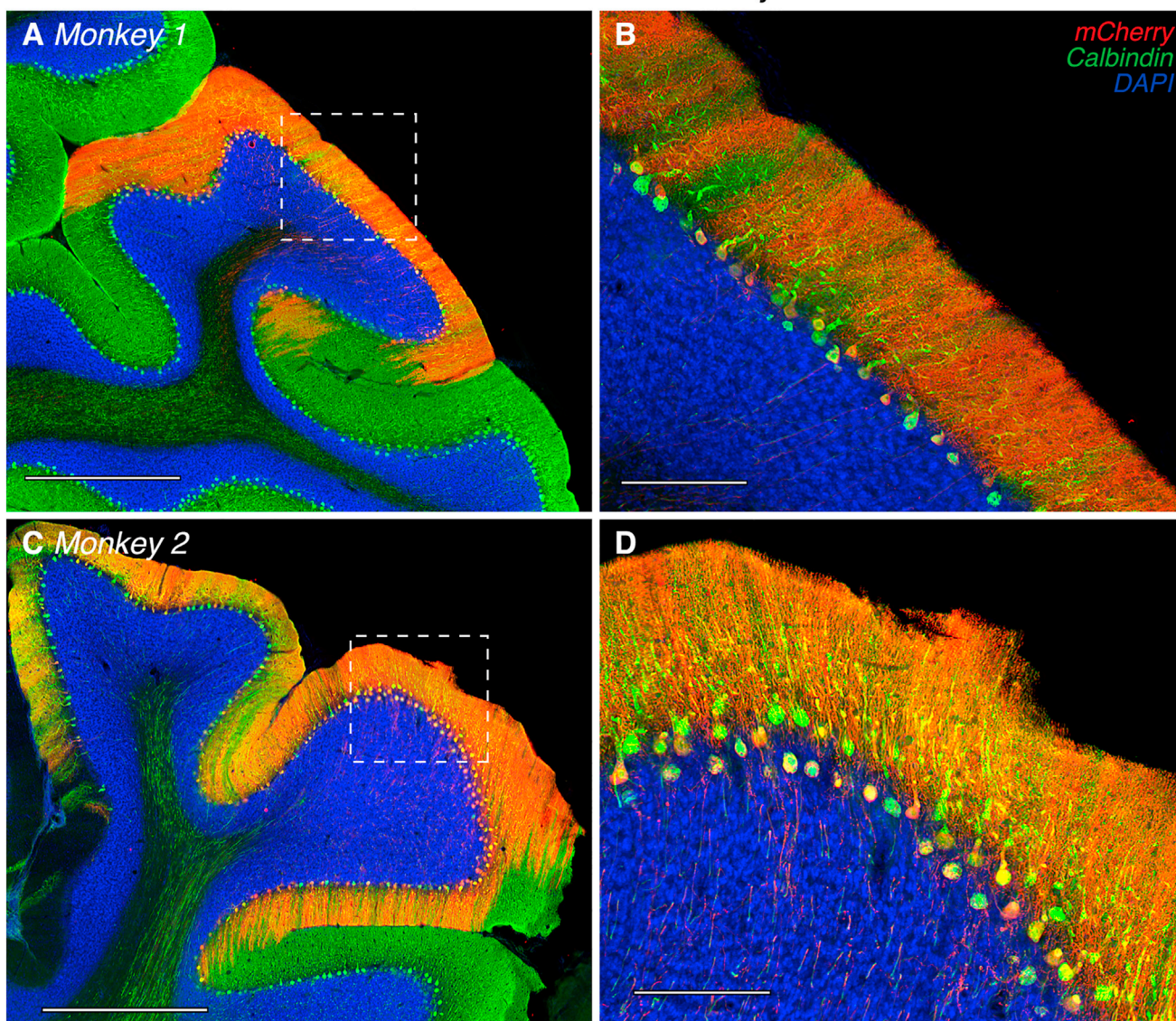


Figure 2. Transduction Pattern of AAV9-L7-ChR2-mCherry

(A and C) 10 \times montages of histological sections from monkey 1 and monkey 2. Scale bars represent 1,000 μ m.

(B and D) 20 \times montages of the sections in (A) and (C) corresponding to regions outlined by the dashed white boxes. Scale bars represent 200 μ m. Most of the mCherry labeling in the granule cell layer is due to Purkinje cell axons.

stimulation in interleaved trials (Figure 5A). We quantified response entrainment at each frequency, fitted these data with a descriptive function, and extracted two parameters: the preferred frequency and high-frequency cutoff (Figure 5B). The preferred frequency of the example unit was 5 Hz (dark gray), and the high-frequency cutoff was 24 Hz (light gray).

Similar results were obtained from other units. Thirty of 31 units fired more spikes during laser trials than control trials (Figure 5C). For 21 of these units, we measured the frequency dependence of optical stimulation up to 500 Hz. The average increase in spiking activity was 2-fold across all frequencies tested and was 17-fold at the preferred frequency (Figure 5D). Preferred

stimulation frequencies ranged from 2 to 14 Hz (median 5 Hz), and high-frequency cutoff values ranged from 3 to 63 Hz (median 19 Hz; Figure 5E). These data demonstrate the reliability of optogenetic activation over a broad range of stimulation frequencies.

Most units responded to light onset with a sustained increase in firing rate but did not entrain to modulations above 100 Hz. We therefore used these high-frequency stimulation conditions to estimate neuronal response latencies to light steps. The latency of optogenetic activation for the example unit was 4 ms. Across the units tested ($n = 16$), latencies ranged from 3 to 59 ms, with a median of 9 ms (Figure 5F). The two units with the longest latencies responded to optical stimulation with slowly ramping

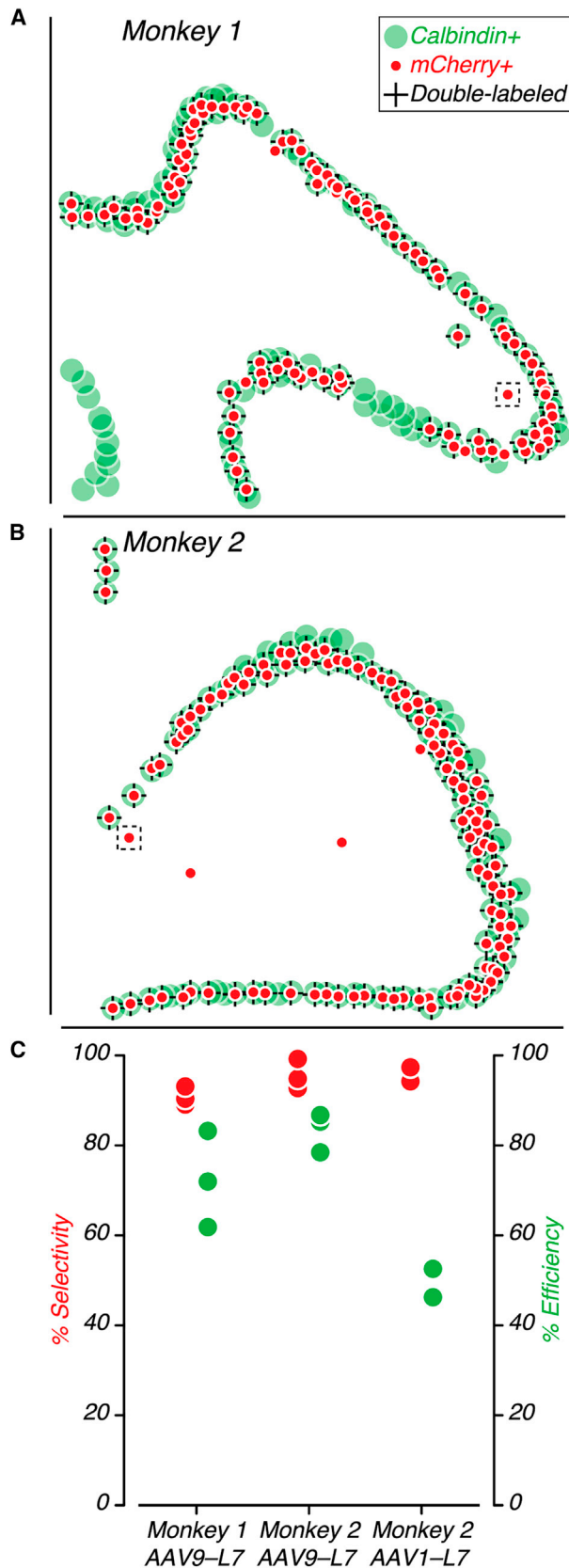


Figure 3. Selectivity and Efficiency of Transduction

(A and B) Schematic of cell counts for two histological sections (same as in Figure 2). Symbols represent calbindin-positive (green), mCherry-positive (red), and double-labeled (“+”) cells. Regions outlined by the dashed black boxes are shown in Figure S1.

(C) Selectivity (left ordinate, red) and efficiency (right ordinate, green) values for each histological section examined.

increases in firing rate, consistent with a polysynaptic response. These units may have been molecular layer interneurons that were disinhibited through activation of Purkinje cell axon collaterals (Witter et al., 2013).

Optogenetic Control of Oculomotor Behavior

To probe the behavioral impact of Purkinje cell activation, we injected monkey 4 with AAV9-L7-ChR2 in the oculomotor vermis (OMV), a midline cerebellar region identified on the basis of saccade-related bursts of neural activity (Figure S4A). The effects of optical stimulation were assessed during visually guided saccades. On each trial, a target appeared 10° away from the fixation point along one of the cardinal directions, and on a random 50% of trials, optical stimulation was triggered by saccade initiation (Figure 6A). An example dataset from one session demonstrates the effect of stimulation on saccade trajectories (Figure 6B). Optical stimulation biased saccade endpoints to the left: rightward saccades became hypometric by 17%, and leftward saccades became hypermetric by 11%. Upward and downward saccades were also biased leftward. Additionally, downward saccades became hypermetric, an effect consistent with protraction of the saccade deceleration phase (Figures S4B–S4E).

We made a total of 11 penetrations through the OMV and encountered light-driven responses in all of them. We conducted behavioral testing at ten of these sites and obtained similar results each time (Figure 7A, colored lines); optical stimulation shifted saccade endpoints leftward and downward. Endpoint shifts depended on saccade direction; downward saccades were shifted predominantly downward, and rightward saccades were shifted predominantly leftward. All shifts were significant except for upward and downward saccades at two stimulation sites (randomization tests, $p < 0.05$; see STAR Methods). The shift direction was correlated across downward, rightward, and leftward saccades (Spearman’s r , $p < 0.1$ for all three pairwise comparisons; e.g., downward versus rightward). This effect was related to the position of the fiber in the OMV (Figure 7A, inset black box). At the rightmost stimulation site, saccade displacement vectors were predominantly downward. As the fiber was moved to the left, saccade displacement vectors rotated clockwise (Spearman’s r between the medio-lateral position of the fiber and the angle of saccade displacement vector, $p < 0.1$ for all three pairwise comparisons).

For each behavioral session, we estimated the time at which saccade trajectories started to differ between control and laser trials from velocity profiles (see STAR Methods). Latency was 14.5 ± 0.4 ms (mean \pm SE) and did not depend on saccade direction or stimulation site (Kruskal-Wallis tests, $p > 0.1$, Figure 7B).

For one well-isolated OMV Purkinje cell, extracellular voltages were sampled at 50 kHz, allowing us to distinguish simple from complex spikes, the hallmark voltage waveforms of Purkinje

AAV1-CMV-GFP

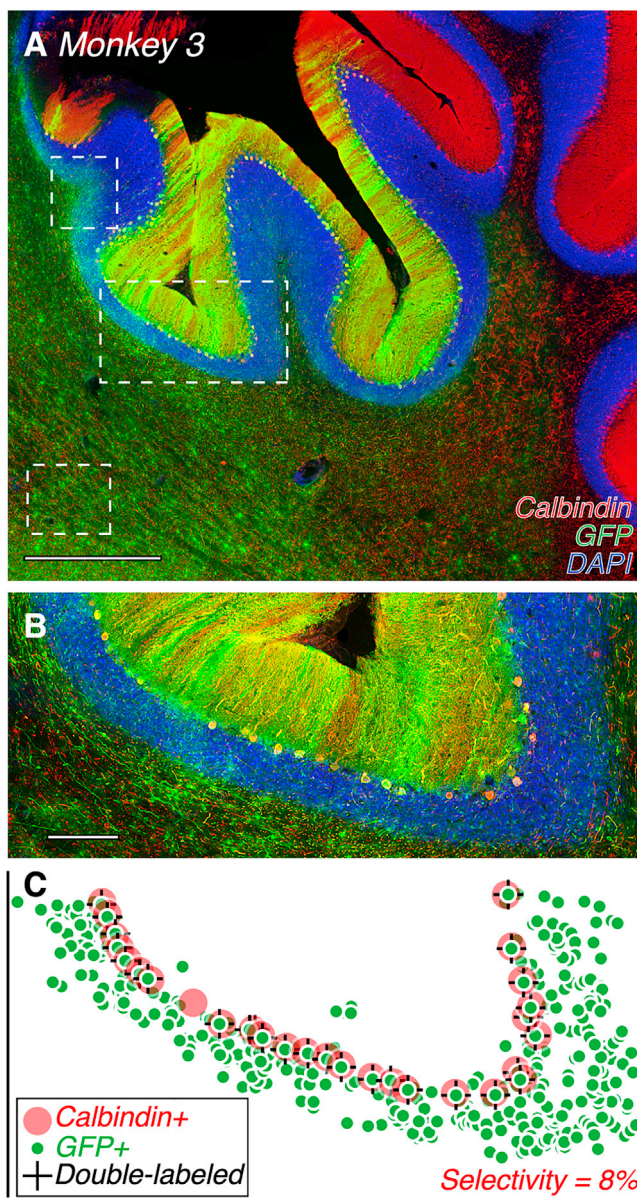


Figure 4. Transduction Pattern of AAV1-CMV-GFP

(A) 10 \times montages of a histological section from monkey 3. Scale bar represents 1,000 μ m.

(B) 20 \times montages of the section in (A), corresponding to the region outlined by the largest dashed white box. Scale bar represents 200 μ m. Regions outlined by the smaller dashed white boxes are shown in Figure S3.

cells (Figure S5). The rate of simple spikes increased during optical stimulation and entrained to square-wave 50 Hz laser pulses (Figure S5A, gray ticks in rasters). The rate of complex spikes, which were identified manually on the basis of waveform (see for example Figure S5B, black circles), also increased during and after optical stimulation (Figure S5A, black circles) but did not entrain to light pulses.

DISCUSSION

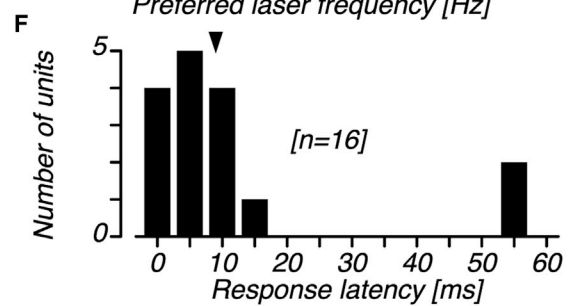
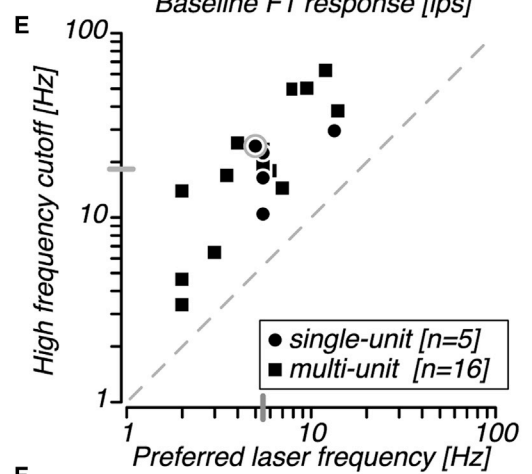
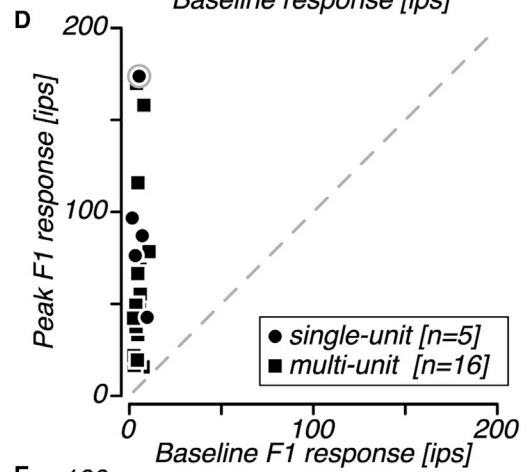
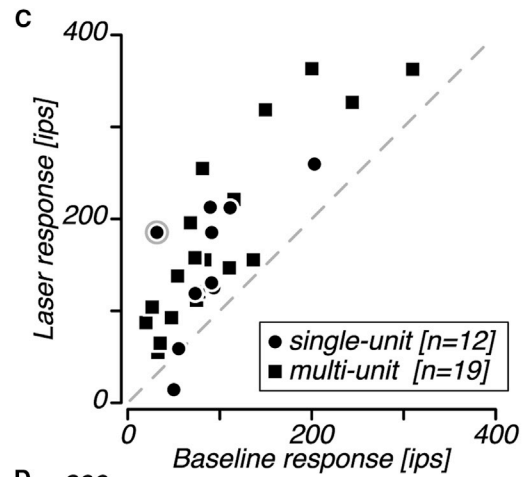
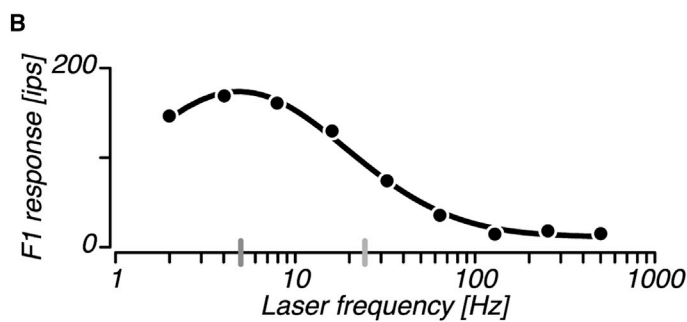
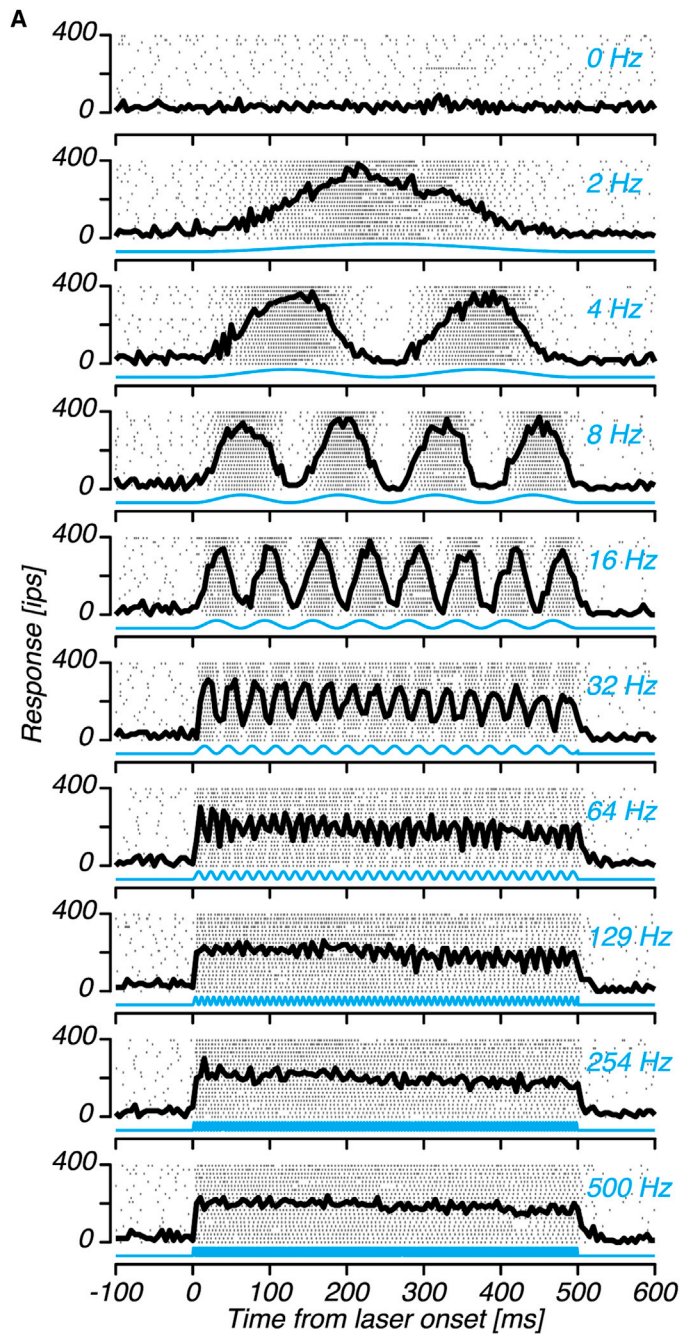
We constructed and vetted a viral vector (AAV-L7-ChR2) for the selective optogenetic activation of cerebellar Purkinje cells in rhesus macaques. Purkinje cell specificity was due to the promoter (compare Figures 2 and 4), not the AAV serotype (Figure 3; Table 1). Optical stimulation caused spiking activity (Figure 5) and consistent changes in saccade endpoints (Figure 7). Thus, AAV-L7-ChR2 enables selective and powerful activation of Purkinje cells, making it an effective tool for investigating their contributions to primate brain function and behavior. Below, we relate our findings to previous efforts to target neuronal types in primates using cell-type-specific promoters in viral vectors. We then discuss applications of this optogenetic tool for studies of cerebellar function.

Promoter-Based Targeting of Cell Types in Primates

A key result of our study is that Purkinje cells of the monkey cerebellum can be transduced selectively by AAV vectors carrying a 1 kb L7 promoter. Such specificity is unusual for viral vector-mediated gene delivery in primates. The modest payload of viral vectors and the presumed length of cell-type-specific promoters challenge the feasibility of this approach, and several attempts to achieve targeting in this way have yielded only moderate specificity (Delzor et al., 2012; Klein et al., 2016; Kügler, 2015; Nathanson et al., 2009a). However, the present study shows that some types of primate neurons can be targeted with precision using short promoters, complementing recent promising efforts described below.

Cell-type-specific promoters have been used to achieve targeted transduction in non-human primates with varying degrees of success. A *CamKII α* promoter (1.3 kb) in an AAV vector was used to activate koniocellular projections from the macaque lateral geniculate nucleus to primary visual cortex, achieving a specificity of 54%–88% (Klein et al., 2016). A TH promoter (3.1 kb) in a lentiviral vector was used to target dopaminergic neurons of macaques, achieving a specificity of 96% (Lerchner et al., 2014). A shorter TH promoter (300 bp) was used in an AAV vector to drive ChR2 expression in this same neuronal type, achieving a specificity of 95% and mediating physiological and behavioral effects (Stauffer et al., 2016). A short, highly conserved gene-regulatory sequence (Dlx, 530 bp) was used to drive GFP expression in GABAergic neurons of marmosets, achieving a specificity of 93% (Dimidschstein et al., 2016). These studies, together with our current findings, provide growing support for the feasibility and promise of viral vector-mediated gene delivery to targeted neuronal classes in primate using short, cell-type-specific promoters.

Our study makes three new contributions to this body of work. First, we showed for the first time that a cell-type-specific promoter can drive sufficient ChR2 expression to mediate robust neuronal responses and changes in behavior. Previously, Stauffer and colleagues (2016) used a cell-type-specific promoter to drive expression of Cre recombinase, which in turn, catalyzed ChR2 expression. The modularity of the Cre-dependent approach permits the use of longer promoter sequences but requires individual neurons to be transduced by two vector particles: one carrying the Cre recombinase gene and another carrying the ChR2 gene. The



(legend on next page)

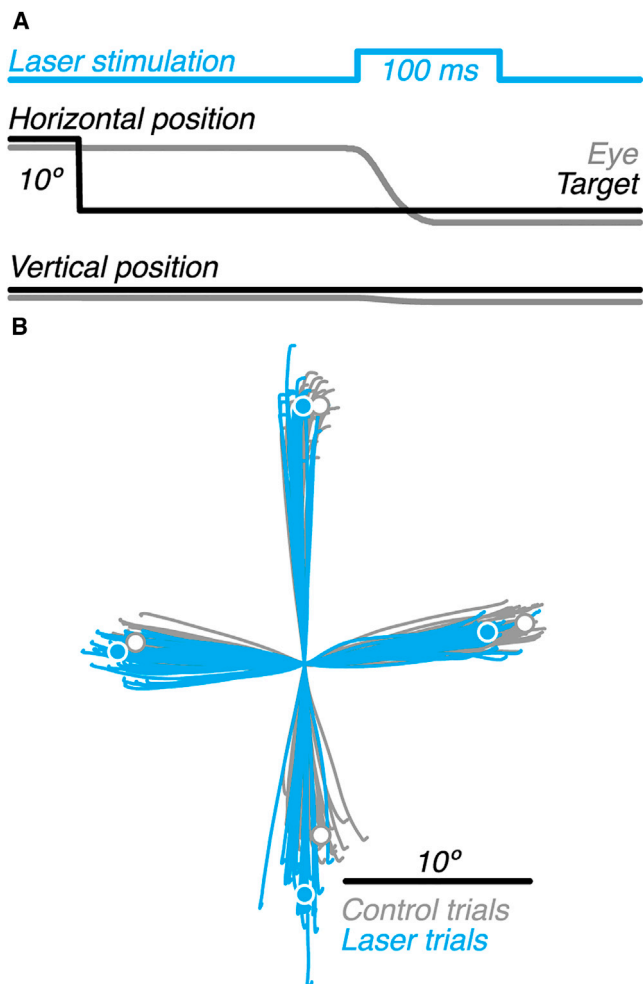


Figure 6. Effect of OMV Stimulation on Saccade Trajectories from One Behavioral Session

(A) Timing of trial events.
 (B) Example saccade trajectories (lines) for control (gray) and laser (blue) trials from a representative stimulation site. Circles represent average saccade endpoints.

requirement for coincident transduction reduces efficiency compared to the single vector approach we used. Second, we showed that a cell-type-specific promoter can be equally selective when packaged in different, distantly related AAV capsids. Third, we showed that cell-type-specific optogenetic manipulation can affect behavior on the timescale of tens of milliseconds. This result contrasts with the use of optogenetics as a means to reinforce a learned behavior across trials (Stauffer et al., 2016).

Figure 5. Optogenetic Activation of Cerebellar Units

(A) Rasters (tick marks) and PSTHs (black) for an example single unit tested with nine frequencies of sinusoidal light modulation (blue).
 (B) Response dependence on stimulation frequency for the same example unit. The curve is a fit to the data (see STAR Methods).
 (C) Strength of optogenetic activation across all frequencies tested.
 (D) Strength of optogenetic activation at the preferred frequency.
 (E) Preferred frequencies and high-frequency cutoff values. The gray bars passing through the ordinate and abscissa mark the median values across all units. Data for the example unit are encircled in gray in (C)–(E). The dashed line represents the identity line.
 (F) Latency of optogenetic activation. Distribution of latencies derived from the responses to 100–500 Hz stimulation. The median latency was 9 ms (triangle).

We conclude that the precise temporal control afforded by optogenetics can be exploited to manipulate signals carried by primate Purkinje cells, a population of neurons for which spike timing is thought to be critical for normal function (De Schutter and Steuber, 2009; Hong et al., 2016).

Potential Applications of AAV-L7-ChR2

Purkinje cell spike trains have structure on multiple timescales (Bell and Grimm, 1969; De Zeeuw et al., 2008), and deciphering this temporal code will require tools that modulate Purkinje cell activity rapidly and reliably. The kinetic properties of the opsin we used, ChR2 (H134R), are ill-suited for high-frequency manipulations (Tchumatchenko et al., 2013). Nevertheless, Purkinje cell responses did entrain faithfully to modulations in the 1–20 Hz range, which subsumes the frequencies produced during sinusoidal oculomotor pursuit, as well as vestibular and optokinetic stimulation protocols (Heck et al., 2013; Lisberger and Fuchs, 1978; Miles et al., 1980; Noda and Warabi, 1987; Stone and Lisberger, 1990; Suzuki and Keller, 1988). Almost all of the units we recorded followed sinusoidal optical stimulation closely; one unit had a frequency-doubled response near the preferred frequency (data not shown).

Developing optogenetic technologies that produce activity patterns that mimic natural states will facilitate interpretation of the physiological and behavioral effects that ensue. Opsins with faster kinetics will extend the range of temporal patterns that can be produced in Purkinje cells (Govorunova et al., 2017; Gunaydin et al., 2010; Klapoetke et al., 2014; Lin et al., 2009). Devices that deliver spatially patterned lights (Farah et al., 2015; Zorzos et al., 2012) will broaden the range of useful manipulations further. However, uncertainty about the spatial activity patterns that occur naturally and the convoluted structure of cerebellar cortex make this approach challenging for studying Purkinje cells.

Purkinje cells affect cerebellar output via their projections onto the deep cerebellar nuclei (DCN). However, the relationship between activity in Purkinje cells and their DCN targets is not well understood. Purkinje cells inhibit DCN neurons (Chan-Palay et al., 1982; Ito et al., 1964) but these two neuronal populations do not always modulate reciprocally (McDevitt et al., 1987), owing presumably to other inputs to the DCN (Heck et al., 2013). The temporal structure of Purkinje cell spiking is also thought to play an important role; when synchronized, Purkinje cells can increase DCN firing rates through a post-inhibitory rebound mechanism (Czubayko et al., 2001; Gauck and Jaeger, 2000; Person and Raman, 2012). Experiments in which Purkinje cell activation is combined with simultaneous recordings of DCN neurons may reveal how different temporal patterns of Purkinje cell spiking modulate DCN activity. Additionally, optogenetic

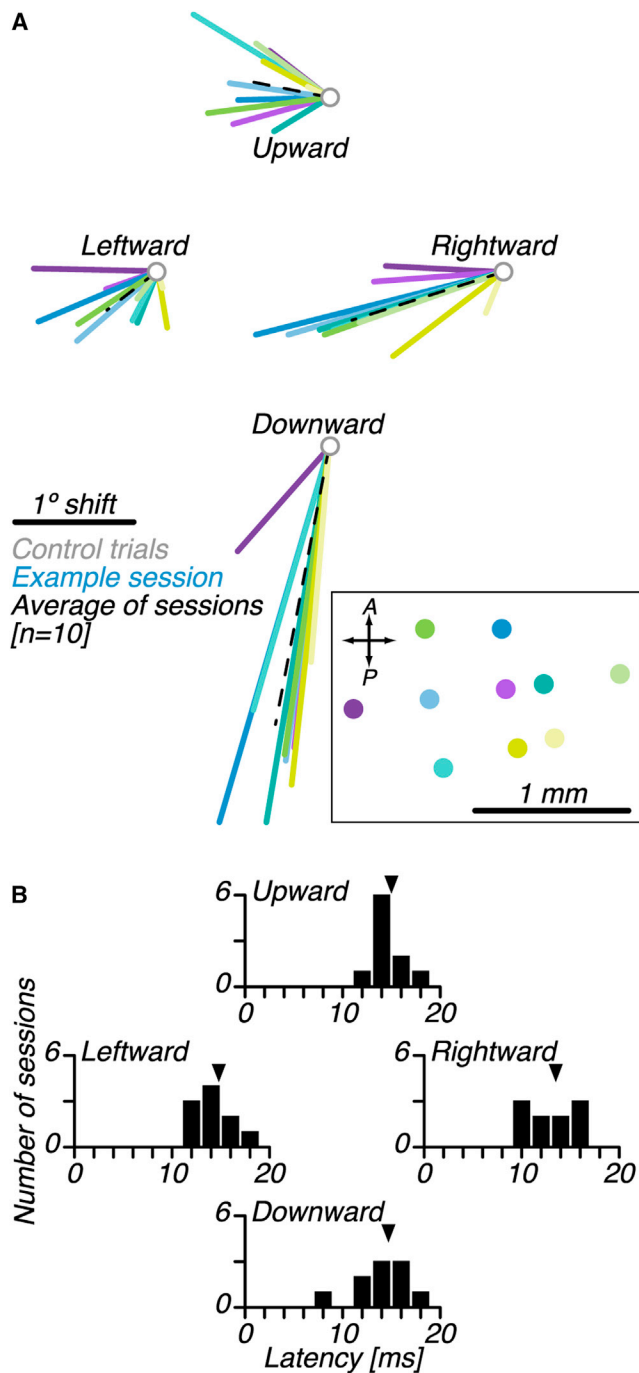


Figure 7. Effect of OMV Stimulation on Saccade Trajectories from All Behavioral Sessions

(A) Average changes in saccade end point for each stimulation site ($n = 10$ stimulation sites, colored lines) and across sites (dashed line). Inset (black box) shows the location of stimulation sites within the recording chamber in the same color code.

(B) Latency of the first significant change in saccade velocity (see STAR Methods).

activation of Purkinje cells during movements that modulate mossy fiber activity (Kase et al., 1980; Ohtsuka and Noda, 1992; Prsa et al., 2009; van Kan et al., 1993) may provide new insights into the interactions among pathways.

To investigate information transfer from Purkinje cells to DCN neurons directly, Purkinje cells can be stimulated optically at their axon terminals. This approach has the advantages of stimulating only the subset of Purkinje cells that innervate a region of interest in the DCN and facilitating postsynaptic response measurement. The dense axonal ChR2-mCherry expression we observed in the dentate nucleus (Figure S6), and previous successes in activating axon terminals in primates (El-Shamayleh et al., 2016; Galvan et al., 2016; Inoue et al., 2015; Klein et al., 2016), augur well for this approach.

The DCN inhibits the inferior olive, which in turn excites Purkinje cells, creating an olivo-cerebellar loop. Signals in this circuit may account for the increase in complex spiking that we observed after Purkinje cell activation (Figure S5; also see Chaumont et al., 2013; Miall et al., 1998). The long delay between optogenetic activation and increased complex spiking is consistent with the dynamics of the inhibitory synapse between the DCN and the inferior olive (Best and Regehr, 2009).

Effects of OMV Purkinje Cell Activation during Saccades

We investigated the effect of Purkinje cell activation on saccades, a behavior that is tightly regulated by the cerebellum (Kheradmand and Zee, 2011; Robinson and Fuchs, 2001). Optical stimulation of Purkinje cells in the OMV produced robust and consistent saccade dysmetria. The robustness of this effect may be due to the fact that even modest variability in Purkinje cell firing rates can manifest in oculomotor behavior (Chaisanguanthum et al., 2014; Medina and Lisberger, 2007). The consistency of the effect suggests that optical stimulation excited populations of Purkinje cells that project to a common region of the DCN, in agreement with the coarse topography of the OMV over the region we sampled (Noda and Fujikado, 1987; Ohtsuka and Noda, 1995). Our data support the idea that Purkinje cells in the OMV contribute to saccades via projections to their DCN target—the caudal fastigial nucleus (cFN)—and subsequent influence on the brainstem (Kojima et al., 2014, see their Figure 8).

Optical stimulation of OMV Purkinje cells in monkey 4 caused robust responses that waned after 4 months of experimentation. Histological analyses revealed Purkinje cell-specific death in monkey 4 (Figure S4A). This cell death was presumably due to our experimental procedures. Mechanical damage, excitotoxicity, phototoxicity, and toxicity from overexpression all may have contributed (Choi, 1987; Frigault et al., 2009; Hirase et al., 2002; Miyashita et al., 2013; Stubblefield et al., 2013; Yizhar et al., 2011). Teasing these factors apart will require experiments in which optical fiber insertion, light delivery, and opsin expression are dissociated. We note that monkey 4 was euthanized 6 months after injection, whereas the next-longest duration for the other monkeys was 3 months, consistent with the idea that cell death occurred several months after vector injection.

Optical stimulation of OMV Purkinje cells failed to evoke saccades, in contrast to electrical stimulation (Fujikado and

Table 1. Estimates of Position and Extent of Transduced Cerebellar Regions

Monkey	Vector	Lobule	Spread (Anterior–Posterior) (mean ± SD)	Position (Medial–Lateral)	Spread (Medial–Lateral)
1	AAV9–L7	IIIb	2.4 ± 0.1 mm	~6 mm	~5 mm
2	AAV9–L7	II	3.1 ± 0.1 mm	~3 mm	~10 mm
2	AAV1–L7	IIIb, IVa	1.9 ± 0.2 mm	~2 mm	~2 mm
3	AAV1–CMV	Vd, Ve, Vf	5.1 ± 0.5 mm	~8 mm	~5 mm
4	AAV9–L7	VIc, VII, VIIIa	6.7 ± 0.8 mm	~0 mm	~8 mm ^a

Lobules were identified based on an anatomical atlas of the rhesus monkey cerebellum (Madigan and Carpenter, 1971).

^apatchy expression

Noda, 1987; McElligott and Keller, 1984; Noda and Fujikado, 1987; Ron and Robinson, 1973). This finding is consistent with reports of optogenetic stimulation affecting primate behavior more weakly than electrical stimulation does (Cavanaugh et al., 2012; Diester et al., 2011; Han, 2012; Han et al., 2009; Ohayon et al., 2013). Explanations for this difference include that optical stimulation activates neurons over relatively short distances (Histed et al., 2009), evokes only low-frequency spiking in ChR2-positive axons (Hass and Glickfeld, 2016; Jackman et al., 2014), and does not activate afferents antidromically. Additionally, to evoke a saccade, stimulation must be strong enough to suppress omnipause neurons in the brainstem (Fuchs et al., 1985), whereas weaker stimulation is sufficient to bias saccade metrics (Keller et al., 1983; Ohtsuka and Noda, 1991).

Mid-flight optical stimulation of OMV Purkinje cells biased visually guided saccades leftward. This result implies that stimulation was delivered to the left OMV and is consistent with previous studies that used other techniques: electrical stimulation (Fujikado and Noda, 1987; Keller et al., 1983; McElligott and Keller, 1984; Noda and Fujikado, 1987; Ron and Robinson, 1973) and pharmacological manipulation of the OMV (Kojima et al., 2010) and the cFN (Iwamoto and Yoshida, 2002; Robinson et al., 1993; Straube et al., 2009). We found additionally that optogenetic stimulation caused downward saccades to become hypermetric. Dysmetria of upward and downward saccades has been observed in previous studies but was not emphasized perhaps due to the variability of these effects (Iwamoto and Yoshida, 2002; Keller et al., 1983; Straube et al., 2009). We speculate that the consistency in downward hypermetria we observed was due to consistency in the Purkinje cell population stimulated optically.

Apart from being useful for oculomotor neurophysiology, Purkinje cell-specific optogenetics in primates may reveal contributions to non-motor capacities—a controversial aspect of cerebellar function (Baumann et al., 2015; Buckner, 2013; Schmahmann, 2010; Strick et al., 2009). Patients with cerebellar lesions do not exhibit gross cognitive deficits (Frank et al., 2007; Richter et al., 2005; Timmann and Daum, 2007), but convergent evidence suggests that Purkinje cell dysfunction contributes to autism spectrum disorders (Reeber et al., 2013) and schizophrenia (Andreassen and Pierson, 2008). The cerebellum has also been implicated in visual motion perception (Händel et al., 2009), interval timing (Ivry and Keele, 1989), and sequence recognition (Braitenberg et al., 1997; Molinari et al., 2008). Exper-

iments that combine the efficacy and specificity of the AAV–L7–ChR2 vector with the sophisticated behavioral capacities of non-human primates are now poised to reveal Purkinje cell contributions to these behaviors.

STAR★METHODS

Detailed methods are provided in the online version of this paper and include the following:

- KEY RESOURCES TABLE
- CONTACT FOR REAGENT AND RESOURCE SHARING
- EXPERIMENTAL MODEL AND SUBJECT DETAILS
- METHOD DETAILS
 - AAV plasmid engineering and vector production
 - AAV vector injections
 - Neurophysiology
 - Behavior
 - Histology
- QUANTIFICATION AND STATISTICAL ANALYSIS
 - Neurophysiology
 - Behavior
 - Histology

SUPPLEMENTAL INFORMATION

Supplemental Information includes six figures and can be found with this article online at <http://dx.doi.org/10.1016/j.neuron.2017.06.002>.

AUTHOR CONTRIBUTIONS

Y.E.-S., Y.K., R.S., and G.D.H. contributed to study conceptualization, investigation, and analysis. Y.E.-S. and G.D.H. drafted the manuscript. Y.E.-S., Y.K., R.S., and G.D.H. edited the manuscript.

ACKNOWLEDGMENTS

We thank Leah Tait and Skyler Mendoza for assistance with cloning and viral vector production, Michael Shadlen for helpful comments on the manuscript and sharing resources for viral vector production and control data collection, Christopher Fetsch and Mehdi Sanayei for help acquiring control data, Elizabeth Buffalo for generous microscope access, Rachel Wong and Anita Disney for advice on cell counting, Jing Huang for guidance in immunohistochemistry, and Daniel Possin and James Kuchenbecker for guidance in histological image processing and confocal microscopy. We also thank Yoshihiro Yoshihara for the pBstN–L7–WGA plasmid and Karl Deisseroth for the pAAV–hSyn–ChR2–mCherry plasmid. This work was funded by R21EY024362 grant to G.D.H., R01EY019258 to R.S., R01EY023277 to Y.K., R01EY011378 to

Michael Shadlen, NIH/ORIP grant P51OD010425 to the Washington National Primate Research Center, and NEI Center Core Grant for Vision Research P30 EY01730 to the University of Washington.

Received: January 19, 2017

Revised: April 13, 2017

Accepted: June 1, 2017

Published: June 22, 2017

REFERENCES

- Andreasen, N.C., and Pierson, R. (2008). The role of the cerebellum in schizophrenia. *Biol. Psychiatry* *64*, 81–88.
- Baumann, O., Borra, R.J., Bower, J.M., Cullen, K.E., Habas, C., Ivry, R.B., Leggio, M., Mattingley, J.B., Molinari, M., Moulton, E.A., et al. (2015). Consensus paper: the role of the cerebellum in perceptual processes. *Cerebellum* *14*, 197–220.
- Bell, C.C., and Grimm, R.J. (1969). Discharge properties of Purkinje cells recorded on single and double microelectrodes. *J. Neurophysiol.* *32*, 1044–1055.
- Best, A.R., and Regehr, W.G. (2009). Inhibitory regulation of electrically coupled neurons in the inferior olive is mediated by asynchronous release of GABA. *Neuron* *62*, 555–565.
- Braitenberg, V., Heck, D., and Sultan, F. (1997). The detection and generation of sequences as a key to cerebellar function: experiments and theory. *Behav. Brain Sci.* *20*, 229–245, discussion 245–277.
- Buckner, R.L. (2013). The cerebellum and cognitive function: 25 years of insight from anatomy and neuroimaging. *Neuron* *80*, 807–815.
- Calcedo, R., and Wilson, J.M. (2013). Humoral immune response to AAV. *Front. Immunol.* *4*, 341.
- Cavanaugh, J., Monosov, I.E., McAlonan, K., Berman, R., Smith, M.K., Cao, V., Wang, K.H., Boyden, E.S., and Wurtz, R.H. (2012). Optogenetic inactivation modifies monkey visuomotor behavior. *Neuron* *76*, 901–907.
- Chaisanguanthum, K.S., Joshua, M., Medina, J.F., Bialek, W., and Lisberger, S.G. (2014). The neural code for motor control in the cerebellum and oculomotor brainstem. *eNeuro* *1*, 1.
- Chan-Palay, V., Ito, M., Tongroach, P., Sakurai, M., and Palay, S. (1982). Inhibitory effects of motilin, somatostatin, [Leu]enkephalin, [Met]enkephalin, and taurine on neurons of the lateral vestibular nucleus: interactions with gamma-aminobutyric acid. *Proc. Natl. Acad. Sci. USA* *79*, 3355–3359.
- Chaumont, J., Guyon, N., Valera, A.M., Dugué, G.P., Popa, D., Marcaggi, P., Gautheron, V., Reibel-Foisset, S., Dieudonné, S., Stephan, A., et al. (2013). Clusters of cerebellar Purkinje cells control their afferent climbing fiber discharge. *Proc. Natl. Acad. Sci. USA* *110*, 16223–16228.
- Choi, D.W. (1987). Ionic dependence of glutamate neurotoxicity. *J. Neurosci.* *7*, 369–379.
- Czubayko, U., Sultan, F., Thier, P., and Schwarz, C. (2001). Two types of neurons in the rat cerebellar nuclei as distinguished by membrane potentials and intracellular fillings. *J. Neurophysiol.* *85*, 2017–2029.
- De Schutter, E., and Steuber, V. (2009). Patterns and pauses in Purkinje cell simple spike trains: experiments, modeling and theory. *Neuroscience* *162*, 816–826.
- De Zeeuw, C.I., Hoebeek, F.E., and Schonewille, M. (2008). Causes and consequences of oscillations in the cerebellar cortex. *Neuron* *58*, 655–658.
- Delzor, A., Dufour, N., Petit, F., Guillermier, M., Houitte, D., Auregan, G., Brouillet, E., Hantraye, P., and Déglon, N. (2012). Restricted transgene expression in the brain with cell-type specific neuronal promoters. *Hum. Gene Ther. Methods* *23*, 242–254.
- Diester, I., Kaufman, M.T., Mogri, M., Pashaie, R., Goo, W., Yizhar, O., Ramakrishnan, C., Deisseroth, K., and Shenoy, K.V. (2011). An optogenetic toolbox designed for primates. *Nat. Neurosci.* *14*, 387–397.
- Dimidschstein, J., Chen, Q., Tremblay, R., Rogers, S.L., Saldi, G.A., Guo, L., Xu, Q., Liu, R., Lu, C., Chu, J., et al. (2016). A viral strategy for targeting and manipulating interneurons across vertebrate species. *Nat. Neurosci.* *19*, 1743–1749.
- El-Shamayleh, Y., Ni, A.M., and Horwitz, G.D. (2016). Strategies for targeting primate neural circuits with viral vectors. *J. Neurophysiol.* *116*, 122–134.
- Farah, N., Levinsky, A., Brosh, I., Kahn, I., and Shoham, S. (2015). Holographic fiber bundle system for patterned optogenetic activation of large-scale neuronal networks. *Neurophotonics* *2*, 045002.
- Fortin, M., Marchand, R., and Parent, A. (1998). Calcium-binding proteins in primate cerebellum. *Neurosci. Res.* *30*, 155–168.
- Frank, B., Schoch, B., Richter, S., Frings, M., Karnath, H.O., and Timmann, D. (2007). Cerebellar lesion studies of cognitive function in children and adolescents - limitations and negative findings. *Cerebellum* *6*, 242–253.
- Frigault, M.M., Lacoste, J., Swift, J.L., and Brown, C.M. (2009). Live-cell microscopy - tips and tools. *J. Cell Sci.* *122*, 753–767.
- Fuchs, A.F., Kaneko, C.R., and Scudder, C.A. (1985). Brainstem control of saccadic eye movements. *Annu. Rev. Neurosci.* *8*, 307–337.
- Fujikado, T., and Noda, H. (1987). Saccadic eye movements evoked by microstimulation of lobule VII of the cerebellar vermis of macaque monkeys. *J. Physiol.* *394*, 573–594.
- Galvan, A., Hu, X., Smith, Y., and Wichmann, T. (2016). Effects of optogenetic activation of corticothalamic terminals in the motor thalamus of awake monkeys. *J. Neurosci.* *36*, 3519–3530.
- Gao, G., Vandenberghe, L.H., Alvira, M.R., Lu, Y., Calcedo, R., Zhou, X., and Wilson, J.M. (2004). Clades of Adeno-associated viruses are widely disseminated in human tissues. *J. Virol.* *78*, 6381–6388.
- Gauck, V., and Jaeger, D. (2000). The control of rate and timing of spikes in the deep cerebellar nuclei by inhibition. *J. Neurosci.* *20*, 3006–3016.
- Govorunova, E.G., Sineshchekov, O.A., Rodarte, E.M., Janz, R., Morelle, O., Melkonian, M., Wong, G.K., and Spudich, J.L. (2017). The expanding family of natural anion channelrhodopsins reveals large variations in kinetics, conductance, and spectral sensitivity. *Sci. Rep.* *7*, 43358.
- Gunaydin, L.A., Yizhar, O., Berndt, A., Sohal, V.S., Deisseroth, K., and Hegemann, P. (2010). Ultrafast optogenetic control. *Nat. Neurosci.* *13*, 387–392.
- Han, X. (2012). Optogenetics in the nonhuman primate. *Prog. Brain Res.* *196*, 215–233.
- Han, X., Qian, X., Bernstein, J.G., Zhou, H.H., Franzesi, G.T., Stern, P., Bronson, R.T., Graybiel, A.M., Desimone, R., and Boyden, E.S. (2009). Millisecond-timescale optical control of neural dynamics in the nonhuman primate brain. *Neuron* *62*, 191–198.
- Händel, B., Thier, P., and Haarmeier, T. (2009). Visual motion perception deficits due to cerebellar lesions are paralleled by specific changes in cerebro-cortical activity. *J. Neurosci.* *29*, 15126–15133.
- Hanks, T., Kiani, R., and Shadlen, M.N. (2014). A neural mechanism of speed-accuracy tradeoff in macaque area LIP. *eLife* *3*, 27.
- Hass, C.A., and Glickfeld, L.L. (2016). High-fidelity optical excitation of cortico-cortical projections at physiological frequencies. *J. Neurophysiol.* *116*, 2056–2066.
- Hass, C.A., and Horwitz, G.D. (2013). V1 mechanisms underlying chromatic contrast detection. *J. Neurophysiol.* *109*, 2483–2494.
- Heck, D.H., De Zeeuw, C.I., Jaeger, D., Khodakhah, K., and Person, A.L. (2013). The neuronal code(s) of the cerebellum. *J. Neurosci.* *33*, 17603–17609.
- Hirase, H., Nikolenko, V., Goldberg, J.H., and Yuste, R. (2002). Multiphoton stimulation of neurons. *J. Neurobiol.* *51*, 237–247.
- Histed, M.H., Bonin, V., and Reid, R.C. (2009). Direct activation of sparse, distributed populations of cortical neurons by electrical microstimulation. *Neuron* *63*, 508–522.
- Holmes, G. (1939). The cerebellum of man. *Brain Res.* *62*, 1–30.
- Hong, S., Negrello, M., Junker, M., Smilgin, A., Thier, P., and De Schutter, E. (2016). Multiplexed coding by cerebellar Purkinje neurons. *eLife* *5*, 5.

- Horwitz, G.D., and Hass, C.A. (2012). Nonlinear analysis of macaque V1 color tuning reveals cardinal directions for cortical color processing. *Nat. Neurosci.* **15**, 913–919.
- Horwitz, G.D., Batista, A.P., and Newsome, W.T. (2004). Representation of an abstract perceptual decision in macaque superior colliculus. *J. Neurophysiol.* **91**, 2281–2296.
- Iida, A., Takino, N., Miyauchi, H., Shimazaki, K., and Muramatsu, S. (2013). Systemic delivery of tyrosine-mutant AAV vectors results in robust transduction of neurons in adult mice. *BioMed Res. Int.* **2013**, 974819.
- Inoue, K., Takada, M., and Matsumoto, M. (2015). Neuronal and behavioural modulations by pathway-selective optogenetic stimulation of the primate oculomotor system. *Nat. Commun.* **6**, 8378.
- Ioffe, M.E. (2013). Cerebellar control of posture. In *Handbook of the Cerebellum and Cerebellar Disorders*, M. Manto, D.L. Gruol, J. Schmahmann, N. Koibuchi, and F. Rossi, eds. (Springer), pp. 1221–1240.
- Ito, M. (2002). Historical review of the significance of the cerebellum and the role of Purkinje cells in motor learning. *Ann. N Y Acad. Sci.* **978**, 273–288.
- Ito, M., Yoshida, M., and Obata, K. (1964). Monosynaptic inhibition of the intracerebellar nuclei induced from the cerebellar cortex. *Experientia* **20**, 575–576.
- Ivry, R.B., and Keele, S.W. (1989). Timing functions of the cerebellum. *J. Cogn. Neurosci.* **1**, 136–152.
- Iwamoto, Y., and Yoshida, K. (2002). Saccadic dysmetria following inactivation of the primate fastigial oculomotor region. *Neurosci. Lett.* **325**, 211–215.
- Jackman, S.L., Beneduce, B.M., Drew, I.R., and Regehr, W.G. (2014). Achieving high-frequency optical control of synaptic transmission. *J. Neurosci.* **34**, 7704–7714.
- Jande, S.S., Maler, L., and Lawson, D.E. (1981). Immunohistochemical mapping of vitamin D-dependent calcium-binding protein in brain. *Nature* **294**, 765–767.
- Jazayeri, M., Lindbloom-Brown, Z., and Horwitz, G.D. (2012). Saccadic eye movements evoked by optogenetic activation of primate V1. *Nat. Neurosci.* **15**, 1368–1370.
- Kase, M., Miller, D.C., and Noda, H. (1980). Discharges of Purkinje cells and mossy fibres in the cerebellar vermis of the monkey during saccadic eye movements and fixation. *J. Physiol.* **300**, 539–555.
- Keller, E.L., Slakey, D.P., and Crandall, W.F. (1983). Microstimulation of the primate cerebellar vermis during saccadic eye movements. *Brain Res.* **288**, 131–143.
- Kheradmand, A., and Zee, D.S. (2011). Cerebellum and ocular motor control. *Front. Neurol.* **2**, 53.
- Kira, S., Yang, T., and Shadlen, M.N. (2015). A neural implementation of Wald's sequential probability ratio test. *Neuron* **85**, 861–873.
- Klapoetke, N.C., Murata, Y., Kim, S.S., Pulver, S.R., Birdsey-Benson, A., Cho, Y.K., Morimoto, T.K., Chuong, A.S., Carpenter, E.J., Tian, Z., et al. (2014). Independent optical excitation of distinct neural populations. *Nat. Methods* **11**, 338–346.
- Klein, C., Evrard, H.C., Shapcott, K.A., Haverkamp, S., Logothetis, N.K., and Schmid, M.C. (2016). Cell-targeted optogenetics and electrical microstimulation reveal the primate koniocellular projection to supra-granular visual cortex. *Neuron* **90**, 143–151.
- Kojima, Y., Soetedjo, R., and Fuchs, A.F. (2010). Effects of GABA agonist and antagonist injections into the oculomotor vermis on horizontal saccades. *Brain Res.* **1366**, 93–100.
- Kojima, Y., Robinson, F.R., and Soetedjo, R. (2014). Cerebellar fastigial nucleus influence on ipsilateral abducens activity during saccades. *J. Neurophysiol.* **111**, 1553–1563.
- Kügler, S. (2015). Tissue-specific promoters in the CNS. In *Gene Therapy for Neurological Disorders: Methods and Protocols*, F.P. Manfredsson, ed. (Springer), pp. 81–91.
- Lerchner, W., Corgiat, B., Der Minassian, V., Saunders, R.C., and Richmond, B.J. (2014). Injection parameters and virus dependent choice of promoters to improve neuron targeting in the nonhuman primate brain. *Gene Ther.* **21**, 233–241.
- Lin, J.Y., Lin, M.Z., Steinbach, P., and Tsien, R.Y. (2009). Characterization of engineered channelrhodopsin variants with improved properties and kinetics. *Biophys. J.* **96**, 1803–1814.
- Lisberger, S.G., and Fuchs, A.F. (1978). Role of primate flocculus during rapid behavioral modification of vestibuloocular reflex. I. Purkinje cell activity during visually guided horizontal smooth-pursuit eye movements and passive head rotation. *J. Neurophysiol.* **41**, 733–763.
- Madigan, J.C., and Carpenter, M.B. (1971). *Cerebellum of the Rhesus Monkey; Atlas of Lobules, Laminae, and Folia, in Sections* (University Park Press).
- McDevitt, C.J., Ebner, T.J., and Bloedel, J.R. (1987). Relationships between simultaneously recorded Purkinje cells and nuclear neurons. *Brain Res.* **425**, 1–13.
- McElligott, J.G., and Keller, E.L. (1984). Cerebellar vermis involvement in monkey saccadic eye movements: microstimulation. *Exp. Neurol.* **86**, 543–558.
- Medina, J.F., and Lisberger, S.G. (2007). Variation, signal, and noise in cerebellar sensory-motor processing for smooth-pursuit eye movements. *J. Neurosci.* **27**, 6832–6842.
- Mendoza, S.D., El-Shamayleh, Y., and Horwitz, G.D. (2017). AAV-mediated delivery of optogenetic constructs to the macaque brain triggers humoral immune responses. *J. Neurophysiol.* **117**, 2004–2013.
- Miall, R.C., Keating, J.G., Malkmus, M., and Thach, W.T. (1998). Simple spike activity predicts occurrence of complex spikes in cerebellar Purkinje cells. *Nat. Neurosci.* **1**, 13–15.
- Miles, F.A., Braitman, D.J., and Dow, B.M. (1980). Long-term adaptive changes in primate vestibuloocular reflex. IV. Electrophysiological observations in flocculus of adapted monkeys. *J. Neurophysiol.* **43**, 1477–1493.
- Miyashita, T., Shao, Y.R., Chung, J., Pourzia, O., and Feldman, D.E. (2013). Long-term channelrhodopsin-2 (ChR2) expression can induce abnormal axonal morphology and targeting in cerebral cortex. *Front. Neural Circuits* **7**, 8.
- Molinari, M., Chiricozzi, F.R., Clausi, S., Tedesco, A.M., De Lisa, M., and Leggio, M.G. (2008). Cerebellum and detection of sequences, from perception to cognition. *Cerebellum* **7**, 611–615.
- Morton, S.M., and Bastian, A.J. (2004). Cerebellar control of balance and locomotion. *Neuroscientist* **10**, 247–259.
- Nathanson, J.L., Jappelli, R., Scheeff, E.D., Manning, G., Obata, K., Brenner, S., and Callaway, E.M. (2009a). Short promoters in viral vectors drive selective expression in mammalian inhibitory neurons, but do not restrict activity to specific inhibitory cell-types. *Front. Neural Circuits* **3**, 19.
- Nathanson, J.L., Yanagawa, Y., Obata, K., and Callaway, E.M. (2009b). Preferential labeling of inhibitory and excitatory cortical neurons by endogenous tropism of adeno-associated virus and lentivirus vectors. *Neuroscience* **161**, 441–450.
- Ni, A.M., Murray, S.O., and Horwitz, G.D. (2014). Object-centered shifts of receptive field positions in monkey primary visual cortex. *Curr. Biol.* **24**, 1653–1658.
- Noda, H., and Fujikado, T. (1987). Involvement of Purkinje cells in evoking saccadic eye movements by microstimulation of the posterior cerebellar vermis of monkeys. *J. Neurophysiol.* **57**, 1247–1261.
- Noda, H., and Warabi, T. (1987). Responses of Purkinje cells and mossy fibres in the flocculus of the monkey during sinusoidal movements of a visual pattern. *J. Physiol.* **387**, 611–628.
- Oberdick, J., Smeyne, R.J., Mann, J.R., Zackson, S., and Morgan, J.I. (1990). A promoter that drives transgene expression in cerebellar Purkinje and retinal bipolar neurons. *Science* **248**, 223–226.
- Ohayon, S., Grimaldi, P., Schweers, N., and Tsao, D.Y. (2013). Saccade modulation by optical and electrical stimulation in the macaque frontal eye field. *J. Neurosci.* **33**, 16684–16697.
- Ohtsuka, K., and Noda, H. (1991). The effect of microstimulation of the oculomotor vermis on discharges of fastigial neurons and visually-directed saccades in macaques. *Neurosci. Res.* **10**, 290–295.

- Ohtsuka, K., and Noda, H. (1992). Burst discharges of mossy fibers in the oculomotor vermis of macaque monkeys during saccadic eye movements. *Neurosci. Res.* 15, 102–114.
- Ohtsuka, K., and Noda, H. (1995). Discharge properties of Purkinje cells in the oculomotor vermis during visually guided saccades in the macaque monkey. *J. Neurophysiol.* 74, 1828–1840.
- Person, A.L., and Raman, I.M. (2012). Synchrony and neural coding in cerebellar circuits. *Front. Neural Circuits* 6, 97.
- Prsa, M., Dash, S., Catz, N., Dicke, P.W., and Thier, P. (2009). Characteristics of responses of Golgi cells and mossy fibers to eye saccades and saccadic adaptation recorded from the posterior vermis of the cerebellum. *J. Neurosci.* 29, 250–262.
- Raymond, J.L., Lisberger, S.G., and Mauk, M.D. (1996). The cerebellum: a neuronal learning machine? *Science* 272, 1126–1131.
- Reeber, S.L., Otis, T.S., and Sillitoe, R.V. (2013). New roles for the cerebellum in health and disease. *Front. Syst. Neurosci.* 7, 83.
- Richter, S., Schoch, B., Kaiser, O., Groetschel, H., Hein-Kropp, C., Maschke, M., Dimitrova, A., Gizewski, E., Ziegler, W., Karnath, H.O., and Timmann, D. (2005). Children and adolescents with chronic cerebellar lesions show no clinically relevant signs of aphasia or neglect. *J. Neurophysiol.* 94, 4108–4120.
- Robinson, F.R., and Fuchs, A.F. (2001). The role of the cerebellum in voluntary eye movements. *Annu. Rev. Neurosci.* 24, 981–1004.
- Robinson, F.R., Straube, A., and Fuchs, A.F. (1993). Role of the caudal fastigial nucleus in saccade generation. II. Effects of muscimol inactivation. *J. Neurophysiol.* 70, 1741–1758.
- Ron, S., and Robinson, D.A. (1973). Eye movements evoked by cerebellar stimulation in the alert monkey. *J. Neurophysiol.* 36, 1004–1022.
- Schmahmann, J.D. (2010). The role of the cerebellum in cognition and emotion: personal reflections since 1982 on the dysmetria of thought hypothesis, and its historical evolution from theory to therapy. *Neuropsychol. Rev.* 20, 236–260.
- Schnütgen, F., Doerflinger, N., Calléja, C., Wendling, O., Chambon, P., and Ghyselinck, N.B. (2003). A directional strategy for monitoring Cre-mediated recombination at the cellular level in the mouse. *Nat. Biotechnol.* 21, 562–565.
- Stugocka, A., Wiaderkiewicz, J., and Barski, J.J. (2017). Genetic targeting in cerebellar Purkinje cells: an update. *Cerebellum* 16, 191–202.
- Stauffer, W.R., Lak, A., Yang, A., Borel, M., Paulsen, O., Boyden, E.S., and Schultz, W. (2016). Dopamine neuron-specific optogenetic stimulation in rhesus macaques. *Cell* 166, 1564–1571.e6.
- Stone, L.S., and Lisberger, S.G. (1990). Visual responses of Purkinje cells in the cerebellar flocculus during smooth-pursuit eye movements in monkeys. I. Simple spikes. *J. Neurophysiol.* 63, 1241–1261.
- Straube, A., Scheuerer, W., Robinson, F.R., and Eggert, T. (2009). Temporary lesions of the caudal deep cerebellar nucleus in nonhuman primates. Gain, offset, and ocular alignment. *Ann. N Y Acad. Sci.* 1164, 119–126.
- Strick, P.L., Dum, R.P., and Fiez, J.A. (2009). Cerebellum and nonmotor function. *Annu. Rev. Neurosci.* 32, 413–434.
- Stubblefield, E.A., Costabile, J.D., and Felsen, G. (2013). Optogenetic investigation of the role of the superior colliculus in orienting movements. *Behav. Brain Res.* 255, 55–63.
- Suzuki, D.A., and Keller, E.L. (1988). The role of the posterior vermis of monkey cerebellum in smooth-pursuit eye movement control. II. Target velocity-related Purkinje cell activity. *J. Neurophysiol.* 59, 19–40.
- Tchumatchenko, T., Newman, J.P., Fong, M.F., and Potter, S.M. (2013). Delivery of continuously-varying stimuli using channelrhodopsin-2. *Front. Neural Circuits* 7, 184.
- Thach, W.T., Goodkin, H.P., and Keating, J.G. (1992). The cerebellum and the adaptive coordination of movement. *Annu. Rev. Neurosci.* 15, 403–442.
- Timmann, D., and Daum, I. (2007). Cerebellar contributions to cognitive functions: a progress report after two decades of research. *Cerebellum* 6, 159–162.
- Tsubota, T., Ohashi, Y., Tamura, K., Sato, A., and Miyashita, Y. (2011). Optogenetic manipulation of cerebellar Purkinje cell activity in vivo. *PLoS ONE* 6, e22400.
- van Kan, P.L., Gibson, A.R., and Houk, J.C. (1993). Movement-related inputs to intermediate cerebellum of the monkey. *J. Neurophysiol.* 69, 74–94.
- Wang, H.X., and Movshon, J.A. (2016). Properties of pattern and component direction-selective cells in area MT of the macaque. *J. Neurophysiol.* 115, 2705–2720.
- Whitney, E.R., Kemper, T.L., Rosene, D.L., Bauman, M.L., and Blatt, G.J. (2008). Calbindin-D28k is a more reliable marker of human Purkinje cells than standard Nissl stains: a stereological experiment. *J. Neurosci. Methods* 168, 42–47.
- Witter, L., Canto, C.B., Hoogland, T.M., de Grujil, J.R., and De Zeeuw, C.I. (2013). Strength and timing of motor responses mediated by rebound firing in the cerebellar nuclei after Purkinje cell activation. *Front. Neural Circuits* 7, 133.
- Wolpert, D.M., Miall, R.C., and Kawato, M. (1998). Internal models in the cerebellum. *Trends Cogn. Sci.* 2, 338–347.
- Yizhar, O., Fenno, L.E., Davidson, T.J., Mogri, M., and Deisseroth, K. (2011). Optogenetics in neural systems. *Neuron* 71, 9–34.
- Yoshihara, Y., Mizuno, T., Nakahira, M., Kawasaki, M., Watanabe, Y., Kagamiyama, H., Jishage, K., Ueda, O., Suzuki, H., Tabuchi, K., et al. (1999). A genetic approach to visualization of multisynaptic neural pathways using plant lectin transgene. *Neuron* 22, 33–41.
- Zozos, A.N., Scholvin, J., Boyden, E.S., and Fonstad, C.G. (2012). Three-dimensional multiwaveguide probe array for light delivery to distributed brain circuits. *Opt. Lett.* 37, 4841–4843.

STAR★METHODS

KEY RESOURCES TABLE

REAGENT or RESOURCE	SOURCE	IDENTIFIER
Antibodies		
mCherry monoclonal antibody	Clontech	Cat. No. 632543; RRID: AB_2307319
Anti-GFP antibody	Abcam	Cat. No. 13970; RRID: AB_300798
Rabbit anti-Calbindin D-28k	Swant	Cat. No. CB38 RRID: AB_10000340
Donkey anti-mouse IgG (H+L) highly cross-adsorbed secondary antibody, Alexa Fluor 594	Molecular Probes	Cat. No. A21203 RRID: AB_141633
Donkey anti-Rabbit IgG (H+L) highly cross-adsorbed secondary antibody, Alexa Fluor 568	Molecular Probes	Cat. No. A10042 RRID: AB_2534017
Donkey anti-Rabbit IgG (H+L) highly cross-adsorbed secondary antibody, Alexa Fluor 488	Molecular Probes	Cat. No. A21206 RRID: AB_141708
Bacterial and Virus Strains		
Stb3 chemically competent <i>E. coli</i>	Invitrogen	Cat. No. C737303
Experimental Models: Cell Lines		
HEK293T cells	American Type Culture Collection	CRL-3216
Experimental Models: Organisms/Strains		
Rhesus monkeys (<i>Macaca mulatta</i>)	Washington National Primate Research Center	N/A
Oligonucleotides		
Primer: L7 Forward: CAGGTTCCAC GCGTCATGTTGGTTG	Integrated DNA Technologies	sL7-F1
Primer: L7 Reverse: ATCGGATCCC CCTGCACGTGG	Integrated DNA Technologies	sL7-R1
Recombinant DNA		
pAAV-hSyn-ChR2(H134R)-mCherry	Deisseroth Lab (Stanford University)	N/A
pXR1	Samulski Lab (University of North Carolina)	N/A
pXR9	Samulski Lab (University of North Carolina)	N/A
pXX6-80	Samulski Lab (University of North Carolina)	N/A
pL7-tWGA	Yoshihara Lab (RIKEN Brain Science Institute)	N/A
Software and Algorithms		
MATLAB	MathWorks	https://www.mathworks.com/products/matlab.html ; RRID: SCR_001622
Fiji	NIH (ImageJ)	https://imagej.net/Fiji ; RRID: SCR_002285
Spike 2	Cambridge Electronic Design	http://ced.co.uk/products/spkovin ; RRID: SCR_000903
Plexon Sort Client	Plexon	http://www.plexon.com ; RRID: SCR:003170
Plexon Offline Sorter	Plexon	http://www.plexon.com ; RRID: SCR:003170

CONTACT FOR REAGENT AND RESOURCE SHARING

Further information and requests for resources and reagents should be directed to and will be fulfilled by the Lead Contact, Gregory D. Horwitz (ghorwitz@u.washington.edu).

EXPERIMENTAL MODEL AND SUBJECT DETAILS

Four healthy rhesus macaques (*Macaca mulatta*) participated in this study (two of each gender; 7–14 kg; 8–17 years). Monkeys were surgically implanted with a head-holding device and a recording chamber that provided access to the cerebellum. Surgical

procedures, experimental protocols and animal care conformed to the NIH *Guide for the Care and Use of Laboratory Animals* and were approved by the Institutional Animal Care and Use Committee at the University of Washington.

Animal husbandry and housing were overseen by the Washington National Primate Research Center. Monkeys 1, 2 and 3 had ad-libitum access to biscuits (Fiber Plus Monkey Diet 5049, Lab Diet) and controlled daily access to fresh produce and water. Monkey 4 had ad-libitum access to water and controlled daily access to food. When possible, animals were pair-housed and allowed grooming contact. Cages were washed every other week, bedding was changed every day, and animals were examined by a veterinarian at least twice per year.

All four monkeys contributed to previous neurophysiological studies. Monkeys 1 and 2 contributed to studies of the primary visual cortex (Hass and Horwitz, 2013; Horwitz and Hass, 2012; Jazayeri et al., 2012; Ni et al., 2014). Monkey 3 contributed to studies of the lateral intraparietal area (Hanks et al., 2014; Kira et al., 2015). Monkey 4 contributed to studies of the superior colliculus (Y.K. and R.S., unpublished data). Monkey 1 had previously received injections of AAV1-hSyn-ChR2-mCherry into the primary visual cortex. Monkey 2 had previously received injections of AAV1-hSyn-oChIEF-citrine into the frontal eye fields. Monkey 4 had previously received injections of AAV1-hSyn-ChR2-mCherry into the superior colliculus. Monkey 3 was naive to AAV vectors at the time of cerebellar injections.

METHOD DETAILS

Monkeys were not assigned to treatment groups by explicit randomization. No replication was performed except for the injections of AAV9-L7-ChR2-mCherry into monkeys 1, 2, and 4. Experimenters were not blind to the vector injected.

AAV plasmid engineering and vector production

We engineered an AAV plasmid containing a promoter fragment of the Purkinje cell protein-2 (L7/Pcp2) gene (Oberdick et al., 1990; Tsubota et al., 2011; Yoshihara et al., 1999) upstream of an open reading frame consisting of channelrhodopsin-2 (ChR2(H134R)) and mCherry coding sequences (Figure 1). A 1 kb sequence of the L7/Pcp2 promoter was amplified from a template plasmid, pBstN-L7-WGA, using PCR primers: CAGGTTCCACGCGTCATGTTGGTTG (forward) and ATCGGATCCCCCTGCACGTGG (reverse). The PCR product was purified by gel electrophoresis, cut with BamH1 and Mlu1 restriction enzymes, and cloned into the pAAV-hSyn-ChR2(H134R)-mCherry plasmid using these unique restriction sites.

Recombinant AAV vectors were produced using a conventional three-plasmid transient transfection of human embryonic kidney cells (HEK293T, female, unauthenticated) with polyethylenimine (25 kDa, Polysciences) or calcium phosphate. Vectors were harvested and purified by ultracentrifugation through an iodixanol gradient column, exchanged into phosphate buffered saline, and titered using qPCR.

AAV vector injections

After mapping a region of the cerebellar cortex using standard extracellular recording techniques, we injected AAV vectors with a Hamilton syringe attached to a manual pump. Monkey 1 received 15 μL of AAV9-L7-ChR2-mCherry (1.41×10^{13} genomes/mL). Monkey 2 received 17 μL of AAV9-L7-ChR2-mCherry (1.41×10^{13} genomes/mL) and 17 μL of AAV1-L7-ChR2-mCherry (1.53×10^{13} genomes/mL). Monkey 4 received 24 μL of AAV9-L7-ChR2-mCherry (1.41×10^{13} genomes/mL). To provide control data, monkey 3 received 17 μL of AAV1-CMV-GFP (6.95×10^{12} genomes/mL). The AAV1-CMV-GFP vector had a similar titer to the AAV1-L7-ChR2 vector to eliminate effects of discrepant titers on transduction pattern (Nathanson et al., 2009b). In monkeys 1, 2 and 3, we injected 1 μL over 3–5 min and waited 3–5 min between each injection along ~ 10 mm tracks. In Monkey 4, we injected four sites with strong saccade-related spiking activity (~ 0.75 mm apart) at up to 4 depths (1.5–2 μL at each depth over the course of 1 min with ≥ 2 min between injections). The position and extent of transduced cerebellar regions are provided (Table 1).

Neurophysiology

Two to six weeks after injections, we searched for neuronal responses to blue light (450 nm; ~ 60 – 100 mW; sinusoidal or square-wave) delivered to the cerebellum via an optical fiber (300 μm outer diameter; Thor Labs) with a beveled tip (tapered over 400–500 μm) that eased entry through the tentorium. A fiber and a recording electrode (Alpha Omega or FHC) were placed in a guide tube and lowered independently into the brain by microdrive. We did not vary the distance between the electrode and the optical fiber systematically but found that distances of < 500 μm typically produced robust responses whereas distances of > 800 μm never evoked responses. The median distance between the electrode and fiber tips was 400 μm ($n = 21$ sites for which we had detailed positional information). Extracellular spiking activity, eye position signals (measured with scleral search coils) and other behavioral and stimulation timing events were digitized and stored for offline analysis (Plexon MAP system or Cambridge Electronics Design Power 1401 system).

Neurophysiological testing conducted in monkeys 1 and 2 employed sinusoidally modulated optical stimulation ($n = 31$ units; 11 from monkey 1 and 20 from monkey 2). During these sessions, animals fixated a central visual target on a computer screen in return for liquid reward. We recorded spiking activity from single units ($n = 12$) and multiunits ($n = 19$), obtaining qualitatively similar results regardless of waveform isolation quality; we therefore pooled these data.

Behavior

Monkey 4 performed a visually guided saccade task. On each trial, the monkey fixated a 0.25° central target for 800–1000 ms, and when the target was displaced by 10° in one of the four cardinal directions, the monkey made a saccade toward the new target location. On randomly interleaved trials (50%), blue light (450 nm) was delivered to the oculomotor vermis (OMV) via optical fiber 6–9 ms after saccade initiation (when the eye velocity exceeded 15°/s) (Figure 6A). At seven of ten stimulation sites, the laser was pulsed (1.5 ms ON; 333 Hz) at 120 mW for 100 ms (i.e., 60 mW, laser power on average); at the remaining three sites, laser power was constant at 60 mW for 100 ms. Both stimulation protocols yielded qualitatively similar results, which were therefore combined.

Histology

We examined fluorescent protein expression histologically at the conclusion of neurophysiological and behavioral experiments. The number of days between vector injections and euthanasia was: 71 (monkey 1), 85 (monkey 2), 31 (monkey 3) and 182 (monkey 4). Animals were euthanized with an overdose of pentobarbital and perfused through the heart with 4% paraformaldehyde followed by a gradient of sucrose in phosphate buffer (10, 20 and 30%). The brain was extracted and cryoprotected in 30% sucrose. Sagittal sections (50 μm) were cut on a sliding microtome and mounted onto slides. Transduced cells were first localized by inspecting native fluorescence signals. Sections were then stained using primary antibodies against the reporter proteins mCherry (Clontech 632543 RRID: AB_2307319, 1:250) and GFP (Abcam 13970 RRID: AB_300798, 1:1000) and against the Purkinje cell marker calbindin (Swant CB38 RRID: AB_10000340, 1:1000), and using secondary antibodies (Invitrogen Molecular Probes): Alexa 594 (A21203 RRID: AB_141633, 1:400), Alexa 568 (A10042 RRID: AB_2534017, 1:400), Alexa 488 (A21206 RRID: AB_141708 and custom, 1:400) and the nuclear stain DAPI (Invitrogen Molecular Probes D-21490, 1:5000) for visualization by epifluorescence and confocal microscopy.

QUANTIFICATION AND STATISTICAL ANALYSIS

All statistical analyses were performed in MATLAB (MathWorks). All hypothesis testing procedures were non-parametric except for the t tests used to determine the latency of the optical stimulation on saccade velocity (Figure 7B). A test of normality was not performed to confirm the validity of this procedure. The shifts in saccade endpoints due to optical stimulation had directions that were restricted to a small portion of the 0–360° range (Figure 7A), justifying the use of Spearman's rank correlation coefficient to examine relationships among the following variables: saccade target location, direction of the saccade end point shift, and mediolateral position of the optical fiber in craniotomy.

Neurophysiology

For each unit recorded, we analyzed rasters and peri-stimulus time histograms (PSTHs) at each laser modulation frequency (Figure 5A) to derive the summary statistics described below.

To examine the frequency dependence of optogenetic activation, we computed the response amplitude from PSTHs at each of the laser modulation frequencies tested (F1 response) and fitted these responses with a log-Gaussian function (Wang and Movshon, 2016):

$$R(f) = R_0 + A \cdot \exp \left[\frac{-\log \left(\frac{f}{f_p} \right)^2}{2\sigma^2} \right]$$

$R(f)$ is the response to frequency f ; R_0 is a vertical offset term; A is the amplitude; f_p is the preferred frequency and σ is the log-Gaussian width. From this fit, we extracted two parameters: (1) the preferred laser modulation frequency (f_p), corresponding to the maximal response amplitude and (2) the high-frequency cutoff, defined as the highest frequency corresponding to half of the maximal response amplitude. We compared these parameters across the population of units tested with the full range of frequencies, up to 500 Hz (Figure 5E; $n = 21$). We excluded from this analysis units for which the highest frequency tested was 283 Hz ($n = 5$ units), 129 Hz ($n = 2$), 16 Hz ($n = 2$), or 8 Hz ($n = 1$).

To evaluate the magnitude and sign of optogenetic activation, we compared the average firing rate during the first 500 ms of optical stimulation across all frequencies to the same epoch on trials without stimulation (Figure 5C). We also compared the response at the preferred stimulation frequency to the response at the same frequency on trials without stimulation (Figure 5D).

To estimate response latency to an abrupt light step, we pooled responses to 129, 222, 259, and 500 Hz stimulation conditions. We first calculated average baseline activity from the 500 ms preceding light onset and then found the first time after this interval (measured in 1 ms steps) at which average optically driven activity exceeded average baseline activity by three standard deviations. These analyses were restricted to the subset of units that showed an increase in activity of 1.5-fold or higher at these frequencies ($n = 16$; Figure 5E). Pooling across frequencies decreased variability at the expense of a bias toward longer latencies; all stimuli were in sine phase and therefore reached peak intensity 1–4 ms after stimulus onset.

Behavior

To estimate the latency of optical stimulation on saccade trajectories, we identified the first time after stimulation onset that the horizontal or vertical eye velocity differed significantly between stimulation and control trials (t tests, $p < 0.01$). The statistical significance of saccade endpoint shifts was assessed by randomization tests (10,000 resamples; Horwitz et al., 2004).

Histology

We quantified transduction selectivity and efficiency by counting mCherry-positive and calbindin-positive cells in montages imaged at 20X at the region of strongest expression in a total of eight histological sections: three from monkey 1 and five from monkey 2 (Figure 2 and Figure S2; 1031 mCherry-positive cells, 1387 calbindin-positive cells and 966 double-labeled cells). We also counted GFP-positive and calbindin-positive cells in one histological section from monkey 3 (Figure 4; 358 GFP-positive cells, 28 calbindin-positive cells and 28 double-labeled cells). Selectivity was defined as the percentage of mCherry-positive cells (or GFP-positive cells in monkey 3) that were also calbindin-positive. Efficiency was defined as the percentage of calbindin-positive cells that were also mCherry-positive. Efficiency decreases with the size of the cell counting region; we provide a single number to document the proportion of Purkinje cells that were labeled near the injection site.

We estimated the position and size of transduced regions along the anterior–posterior axis of the cerebellum by measuring the extent of fluorescent protein expression within parasagittal histological sections. We estimated the position and size of transduced regions along the medial–lateral axis, which is orthogonal to the plane of sectioning, on the basis of section morphology and the number of 50 μm sections over which fluorescence was detectable (Table 1).